Available online at www.sciencedirect.com

ScienceDirect

Procedia Materials Science 8 (2015) 46 – 55

Procedia Materials Science

www.elsevier.com/locate/procedia

International Congress of Science and Technology of Metallurgy and Materials, SAM - CONAMET 2013

Corrosion of Zr-1Nb and Zr-2.5Nb in 0.1 M LiOH at 343ºC

S. Müller, L. Lanzani*

Comisión Nacional de Energía Atómica, Av. Gral. Paz 1499, 1650 San Martín, Buenos Aires, Argentina

Abstract

The corrosion behavior of Zr-2.5%Nb pressure tube material and Zr-1%Nb aged at 560°C for 4 months has been studied in 0.1 M lithium hydroxide solution at 343ºC. The results were compared with those obtained in steam at 400ºC. In the latter, aged alloys showed better behavior than the non-aged materials, whereas the ageing did neither delay the transition nor reduce the weight gains in 0.1 M lithium hydroxide. Second phase particles of Zr-Nb-Fe and Zr-Fe present in aged Zr-1Nb (α+β) and aged Zr-1Nb α' seem to increase hydrogen uptake during post-transition in 0.1 M lithium hydroxide. Regarding the hydrogen absorption in the post-transition period, Zr-1Nb alloys show better performance than Zircaloy-4.

Selection and peer-review under responsibility of the scientific committee of SAM - CONAMET 2013

Keywords: Zr-1Nb, Zr-2.5Nb, ageing, corrosion, LiOH, hydrogen

1. Introduction

The corrosion kinetics of zirconium alloys is characterized by two periods named pre-transition and post-transition. During the pre-transition the growth of the oxide, which is black, compact and adherent, is controlled by diffusion. The kinetics is parabolic and the rate of hydrogen absorption (H uptake) is low during this period [Cox, 2005].

After a certain time the transition (or "breakaway") occurs, leading to the onset of the post-transition period. This period is characterized by a detriment in the response of the material: the corrosion rate increases (linear regime),

* Corresponding author. Tel.: 54-11-6772-7236; fax: 54-11-6772-7362.
E-mail address: lanzani@cnea.gov.ar

Selection and peer-review under responsibility of the scientific committee of SAM - CONAMET 2013
doi:10.1016/j.mspro.2015.04.047

porosity is developed in the oxide (which gradually ceases to be black and looses adherence) and the hydrogen uptake increases due to deterioration of the oxide barrier layer, [Cox, 2005]. How long the material takes to reach the transition depends on the alloying elements, temperature, chemistry of the corrosive medium, etc.

The alloys M5 (Zr-1wt%Nb-O) and ZIRLO (Zr-1wt%Nb-1wt%Sn-0.1wt%Fe) are used at present as fuel cladding material in High Performance PWRs [Cox, 2005, Sabol et al, 1989]. In these reactors lithium hydroxide is added to the water of the primary circuit to maintain a roughly neutral pH so as to control the transport of ferrous corrosion residues throughout the coolant.

It is known that the corrosion resistance of zirconium alloys is strongly affected by the presence of LiOH concentrations around 0.1 M (or higher), conditions in which the time to reach the transition decreases and the post-transition oxidation rate and H uptake increase [Domizzi et al, 1997, Manolescu et al, 1982, Kass, 1969]. This detrimental behavior triggered by LiOH is denominated "accelerated corrosion".

The LiOH concentration in the primary circuit of High Performance PWRs is around 10^{-4} M, which is three orders of magnitude smaller than the concentration that leads to accelerated corrosion. However, the more severe operating conditions in these reactors (higher fuel burn-up and heat fluxes than in conventional reactors) may result in an enhancement of LiOH concentration inside thick porous oxides grown on zirconium alloys, thus reaching the levels in which accelerated corrosion is possible [Cox, 2005]. Moreover, the high temperature corrosion of Zr-Nb alloys strongly depends on the microstructure. This dependence has been widely studied in water [Jeong et al, 2003, Kim et al, 2004] and in diluted LiOH solutions [Choo et al, 1994, Urbanic et al, 1994]; but studies concerning Zr-Nb alloys and the influence of microstructure in concentrated LiOH solutions have not been reported.

In this work the corrosion of Zr-1%Nb and Zr-2.5%Nb (CANDU pressure tube material) in 0.1 M LiOH at 343ºC has been studied. Different metallurgical conditions of both alloys have been tested, particularly the ones obtained after 4 months ageing at 560ºC. The characterization analysis of the different microstructures is presented. TREX of Zircaloy-4 has also been tested, in order to have a reference material not containing niobium as an alloying element. The corrosion kinetics were compared with those obtained in tests conducted in steam at 400ºC.

2. Experimental Procedure

2.1. Materials and Heat Treatments

The alloys tested were: nuclear grade Zr-1wt%Nb (Zr-1Nb), sections of Zr-2.5wt%Nb pressure tube material (Zr-2.5Nb, PT) and TREX of Zircaloy-4. The niobium and iron content, determined by electron microprobe, in Zr-1Nb were: (1.0 ± 0.1) wt% Nb and (1000 ± 100) wt ppm Fe (impurity). A niobium content of (1.10 ± 0.05) wt% Nb was measured in Zr-1Nb through energy dispersive X-ray fluorescence (EDXRF). The commercial grade Zr-2.5Nb (PT) contained: ~ 2.6 wt% Nb, ~ 500 wt ppm Fe (impurity) and ~ 1000 wt ppm O (impurity). The Zircaloy-4 TREX composition corresponded to the nominal composition of this alloy: Zr-1.5 wt%Sn-0.2 wt%Fe-0.1 wt%Cr. The initial hydrogen content in Zr-1Nb and Zr-2.5Nb (PT) was 6 and 8 wt ppm respectively.

The alloys containing niobium were thermally treated. Prior to the heat treatments, the microstructure of as-received Zr-1Nb consisted of α-Zr phase matrix with the niobium–rich β-Zr phase present at the α-Zr grain boundaries (named Zr-1Nb (α+β)), while Zr-2.5Nb (PT) showed the (α-Zr + β-Zr) biphasic structure characteristic of the pressure tube material: elongated α-Zr grains and filaments of β-Zr phase. The microstructure of Zircaloy-4 TREX was similar to that of the cladding material and consisted of equiaxed α-Zr grains and uniformly distributed precipitates, from 0.1 to 0.4 μm in size, of $Zr(Fe/Cr)_2$ and Zr_3Fe.

Specimens of Zr-1Nb and Zr-2.5Nb were polished with SiC paper down to 1200 mesh, degreased in hot ether together with tantalum sheets, rinsed in deionized water at 80ºC and dried with hot air. Then, they were wrapped with tantalum sheets, sealed under argon gas in quartz capsules and submitted to different heat treatments. A batch of as-received Zr-1Nb (α+β) specimens were homogenized for 30 min at 1000ºC and then quenched in iced water in order to obtain the α´- martensitic structure. Specimens of Zr-1Nb (α+β), Zr-1Nb α´and Zr-2.5Nb (PT) were aged at 560ºC for 120 days, in order to achieve equilibrium conditions [Kim et al., 2005, Tofolon-Masclet et al., 2008].

The microstructure of the alloys was revealed by chemical etching with fluonitric solution on the specimens which had a SiC grinding finish of paper 1200 grid. Zircaloy-4 and Zr-1Nb alloys were etched with a solution of: 50 vol. % deionized water, 47 vol. % HNO_3 and 3 vol. % HF; whereas a solution of 47 vol. % deionized water, 47 vol.

% HNO_3 and 6 vol. % HF was for Zr-2.5Nb (PT). The microstructures were observed by OM, FEGSEM and TEM, while the phases were identified using XRD with Cu radiation ($\lambda_{CuK\alpha1}$ = 0.15406 nm, $\lambda_{CuK\alpha2}$ = 0.154439 nm), EDS-SEM and EDS-TEM.

2.2. Corrosion Tests

Circular-section specimens of 1cm in diameter and 0.2 cm thick were cut from each of the metallurgical conditions of Zr-1Nb alloy: as-received (α+β), α´-martensite, aged (α+β) and aged α´-martensite. Rectangular specimens of (1.5 x 0.8 x 0.1) cm^3 were prepared from Zr-2.5Nb (PT) in the conditions: (α+β) and aged (α+β). These specimens were cut so that the (1.5 x 0.8) cm^2 faces were parallel to the circumferential-axial (CA) face of the pressure tube and the 0.8 cm edges were parallel to the main axis of the tube. Zircaloy-4 specimens of ~ 2.5 cm^2 were prepared from offcuts of 0.2 cm thick Zircaloy-4 TREX.

Prior to the autoclaving tests, all the specimens were polished with SiC paper down to 1200 mesh and pickled with fluonitric solution [Müller and Lanzani, 2013]. After this, they were rinsed in deionized water (κ = 1 μS/cm) at 80ºC in order to eliminate traces of the fluoride ion coming from the pickling bath, dried with acetone and hot air and stored in a desiccator. Later, the specimens were measured with a calliper (accuracy of ± 0.005 mm) and weighed in an analytical balance with an accuracy of 0.01 mg.

The corrosion kinetics tests in 0.1 M LiOH solution at (343 ± 3)°C and equilibrium pressure (135 ± 5) bar were carried out in a 2-liter static autoclave containing a 316L stainless steel liner. Before each test the specimens were hung from a rack and put into the liner which contained 500 ml of 0.1 M LiOH solution. Then, the liner was placed into the autoclave which held 200 ml of deionized water. After the tests, the specimens were rinsed, dried and weighed. Autoclaving tests of different durations were performed determining in each case the weight gain per unit area (Δw) of the specimens. The corrosion kinetics in 0.1 M LiOH at (343 ± 3)°C were compared with those obtained in steam at (400 ± 10)ºC and (103 ± 10) bar, tests performed in accordance with the specifications mentioned in the ASTM G2/G2M-06 standard.

The oxide thickness and the hydride distribution were analyzed in cross-sections samples. For this purpose, small pieces were cut from the autoclaved specimens, embedded in epoxi resin and polished with SiC paper down to 1200 mesh. On these objects, the oxide layer thickness was measured by OM using a graduated eyepiece with an accuracy of 1 μm; around five readings were made along each side. Later, the hydrides were revealed on these polished cross sections by etching in fluonitric solution [Müller and Lanzani (2013)] and were observed by OM.

The hydrogen concentration was determined (by duplicate) using a LECO™ analyzer with an accuracy of ± 10%, in small pieces extracted from the autoclaved specimens. Before hydrogen analysis, these pieces were carefully polished with SiC paper for removing the oxide film, degreased in hot ether and rinsed in deionized water at 80ºC.

The extent of corrosion on the coupons was evaluated analyzing the Δw and hydrogen uptake (%H) values, the visual appearance and thickness of the oxide and the hydride distribution within the metal.

3. Results

The heat treatments applied to Zr-1Nb and Zr-2.5Nb alloys, along with the microstructure obtained and the designation of the specimens are described in Table 1.

Fig. 1 shows micrographs of the Zr-Nb alloys studied. As previously said, the β-Zr phase was located at the α-Zr grain boundaries in as-received Zr-1Nb (α+β) (Fig. 1a), and the ageing of this material produced the transformation of β-Zr into agglomerates of β-Nb, Zr-Nb-Fe and Zr-Fe precipitates (Fig. 1b). The fine needle-shaped microstructure of Zr-1Nb α' is observed in Fig. 1c, while Fig. 1d shows the two different precipitate morphologies present in aged Zr-1Nb α': polyhedral and elongated; β-Nb and Zr-Fe phases were identified by EDS. In this alloy, the distribution of precipitates was more homogeneous than that of aged Zr-1Nb (α+β). The microstructure of Zr-2.5Nb (PT) corresponded to that of the CANDU pressure tubes (Fig. 1e), and the ageing of this alloy produced the transformation of β-Zr into globular β-Nb precipitates aligned to the axial direction of the tube (Fig. 1f). Fig. 2 shows a TEM micrograph of these β-Nb particles with the chemical composition measured by EDS. Iron was not detected in the second phase particles of aged Zr-2.5Nb (PT).

Table 1. Heat treatment and microstructure of Zr-1Nb and Zr-2.5Nb alloys. ♦ characterized by XRD; • characterized by EDS

Alloy	Heat treatment	Microstructure	Designation
Zr-1Nb (1000 wt ppm Fe)	—	α-Zr matrix and β-Zr♦ at the grain boundaries. Phase Zr_3Fe♦?	Zr-1Nb (α+β)
	Ageing at 560ºC for 120 days	α-Zr matrix and polyhedral precipitates (~0.3 μm) of β-Nb♦•, Zr-Nb-Fe• and Zr-Fe•	Aged Zr-1Nb (α+β)
	1000ºC for 30 min, followed by quenching in iced water	Martensitic structure	Zr-1Nb α'
	1000ºC for 30 min, followed by quenching in iced water + ageing at 560ºC for 120 days	α-Zr matrix and a more homogeneous distribution of polyhedral (~ 0.3 μm) and elongated (width ~ 0.03 μm) precipitates of β-Nb• and Zr-Fe•	Aged Zr-1Nb α'
Zr-2.5Nb (PT) (500 wt ppm Fe)	—	Biphasic structure of (α-Zr+β-Zr) characteristic of the pressure tubes	Zr-2.5Nb (PT)
	Ageing at 560ºC for 120 days	α-Zr matrix and globular precipitates of β-Nb♦• (0.1-0.3 μm) aligned along the axial direction of the pressure tube	Aged Zr-2.5Nb (PT)

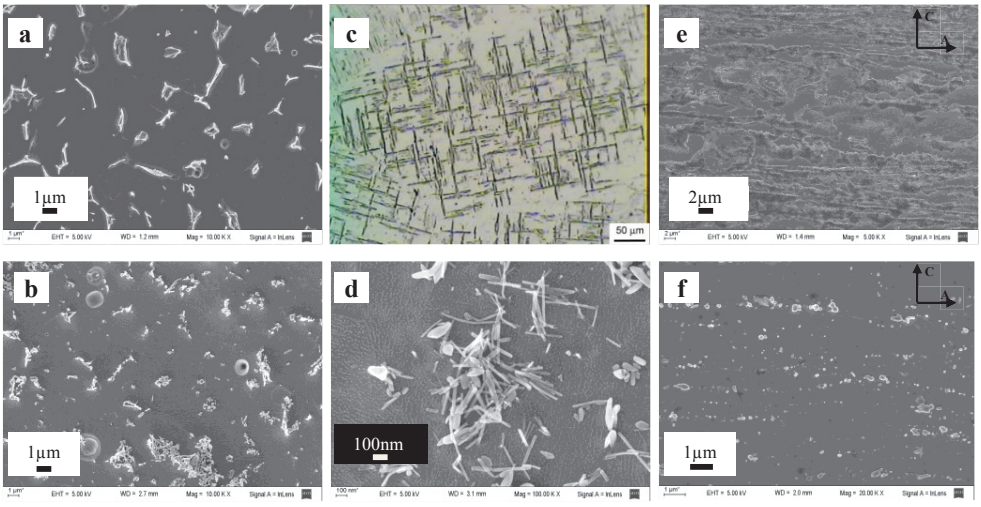

Fig. 1. Micrographs of: (a) as-received Zr-1Nb (α+β), (b) aged Zr-1Nb (α+β), (c) Zr-1Nb α', (d) aged Zr-1Nb α', (e) Zr-2.5Nb, (f) aged Zr-2.5Nb.

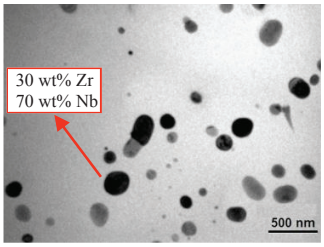

Fig. 2. TEM micrograph showing β-Nb phase in aged Zr-2.5Nb (PT).

Fig. 3a shows the weight gain values Δw (mg/dm^2) obtained for the alloys tested in 0.1 M LiOH at 343°C as a

function of time. All the metallurgical conditions of Zr-1Nb and Zr-2.5Nb showed a pre-transition kinetics up to ~ 2 days exposure. From then on, the "breakaway" occurred ($\Delta w > 60$ mg/dm^2 [Müller and Lanzani, 2013]) and the kinetics changed to a linear rate law. The corrosion rate (v_{corr}) in the linear region was ~ 1.0 mg/dm^{2}h for Zr-2.5Nb and ~ 2.2 mg/dm^{2}h for Zr-1Nb α'; the other alloys exhibited intermediate corrosion rate values (v_{corr} ~ 1.5 mg/dm^{2}h). Although aged Zr-1Nb (α+β) completed the 14-day kinetics, only data within ~ 9 days exposure are shown in Fig. 3a because this alloy suffered oxide flaking (spalling) after the last test, thus having made it difficult to measure the real weight. Unlike niobium containing alloys, Zircaloy-4 did not undergo accelerated corrosion, being the values of Δw ~ 23 mg/dm^2 within ~ 14 days in this medium.

For the sake of comparison, the corrosion kinetics of the alloys in steam at 400ºC and 103 bar are presented in Fig. 3b. Except for Zr-1Nb α', all the other alloys showed a typical pre-transition behavior with weight gains that fit to the equation: $\Delta w = at^b$ (where the exponent b ranges between 0.3 and 0.4). In the case of Zr-1Nb α' alloy, a linear kinetics can be observed from the first Δw value, with a corrosion rate v_{corr} ~ 0.1 mg/dm^{2}h.

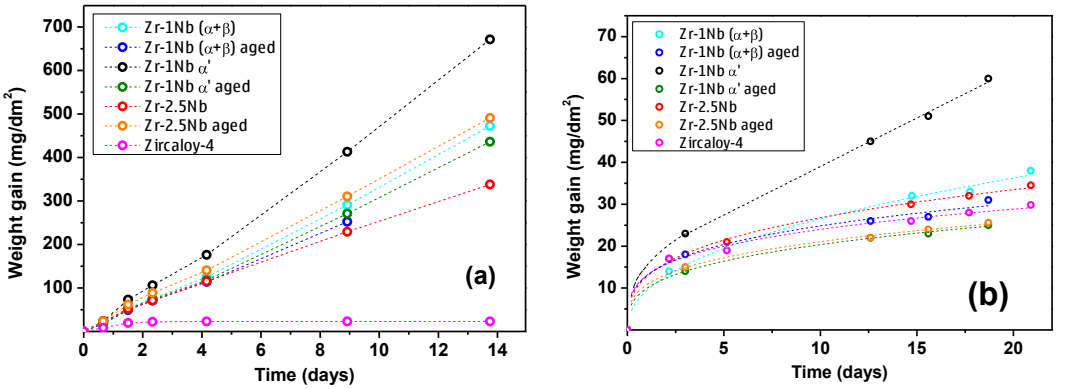

Fig. 3. Corrosion kinetics in: (a) 0.1 M LiOH at 343ºC, (b) steam at 400ºC.

The analysis of the visual appearance of the oxide grown on the alloys after each test pointed out that up to ~ 2 days in 0.1 M LiOH at 343ºC the Zr-1Nb (α+β) and the aged alloys (Zr-1Nb (α+β), Zr-1Nb α' and Zr-2.5Nb) developed adherent oxide layers with a lustrous appearance; The Zr-1Nb α' and Zr-2.5Nb also developed an adherent oxide but with matte appearance. Zircaloy-4 presented an iridescent lustrous black oxide throughout the kinetics. The weight gain value $\Delta w < 28$ mg/dm^2 and the visual appearance of this oxide confirmed that this alloy was in the pre-transition regime even after ~ 14 days in this medium [Müller and Lanzani, 2013]. After ~ 20 days in steam at 400°C, all alloys except Zr-1Nb α' were covered by a uniform black lustrous oxide film, characteristic features of a protective pre-transition oxide. By contrast, the oxide in Zr-1Nb α' was matte and small areas of white oxide were observed at the edges of the specimen.

Table 2 presents the visual appearance of the oxides and the values of: Δw, oxide thickness (d), final hydrogen content [H] and H uptake for all Zr-Nb alloys tested during ~ 14 days in 0.1 M LiOH. The amount of hydrogen absorbed by the specimens (H uptake) was calculated as the percentage (%H) of the total stoichiometric amount of hydrogen liberated by the corrosion reaction $Zr + 2H_2O \rightarrow ZrO_2 + 2H_2$ per unit area of specimen surface. The %H was estimated considering that the hydrogen weight gain was negligible compared to that of oxygen, an approximation that was confirmed with the final results.

Fig. 4 shows the cross-sections of the oxide layers grown on Zr-Nb alloys in 0.1 M LiOH. Oxide layers reached variable thicknesses between 33 and 48 μm in all the niobium alloys, with the exception of aged Zr-1Nb (α+β). The thin oxide thickness (18 μm) measured on this material was related to the oxide spalling (Fig. 4b). Fig. 5a shows the flaking of the oxide layer grown on this material. The difference in contrast observed in polarized light micrographs for oxides in Zr-2.5Nb and in aged Zr-2.5Nb (Figs. 5b and 5c respectively) suggests that the oxide grown on aged PT was more uniform and compact than that on the PT. The same can be observed by comparing Figs. 4e and 4f.

Table 2. Final results after ~ 14 days in 0.1 M LiOH at 343 ºC

Specimen	Appearance of the oxide	Δw (mg/dm^2)	d (μm)	Final [H] (ppm)	H uptake (%H)
Zr-1Nb (α+β)	Beige, opaque	472 ± 3	37 ± 2	82 ± 8	4.0 ± 0.1
Aged Zr-1Nb (α+β)	White, fragile	~330 ± 3 [a]	18 ± 2	270 ± 30	~11 ± 1 [b]
Zr-1Nb α'	Brown, opaque	671 ± 3	48 ± 2	150 ± 20	4.6 ± 0.4
Aged Zr-1Nb α'	Light grey, opaque	436 ± 3	33 ± 2	750 ± 80	13 ± 1
Zr-2.5Nb (PT)	White, friable	338 ± 1	33 ± 2 [c]	46 ± 5	2.9 ± 0.5
Aged Zr-2.5Nb (PT)	Grey, opaque	491 ± 1	36 ± 2 [c]	64 ± 6	3.1 ± 0.1

[a] Extrapolated for ~ 14 days because oxide spalling made it not possible to obtain the Δw after ~ 14 days. [b] Estimated value.
[c] Corresponding to the oxide grown on CA face of the PT.

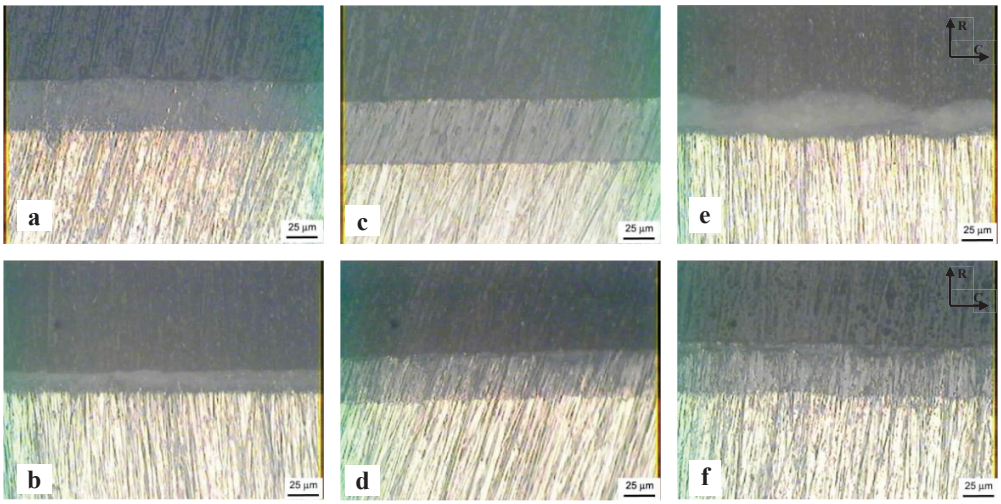

Fig. 4. Oxide cross-sections after ~ 14 days in 0.1 M LiOH at 343ºC: (a) Zr-1Nb (α+β), (b) aged Zr-1Nb (α+β), (c) Zr-1Nb α', (d) aged Zr-1Nb α', (e) Zr-2.5Nb (PT) (oxide on CA face), (f) aged Zr-2.5Nb (PT) (oxide on CA face).

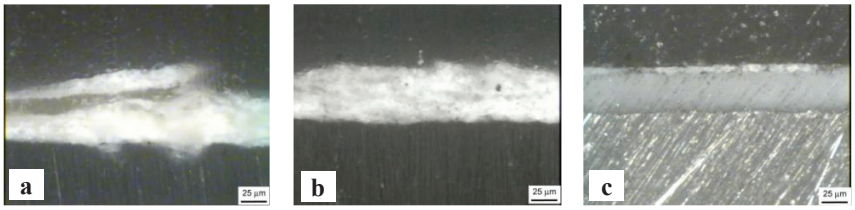

Fig. 5. Polarized light micrographs of the oxide cross-sections for: (a) aged Zr-1Nb (α+β), (b) Zr-2.5Nb (oxide on CA face), (c) aged Zr-2.5Nb (oxide on CA face).

The hydride distributions in the Zr-Nb alloys tested in 0.1 M LiOH, along with the final hydrogen content are shown in Fig. 6. In the case of Zr-1Nb (α+β), it was difficult to distinguish the hydrides platelets from the β-Zr phase in the optical micrographs due to their similar appearances (Fig. 6a), while in aged Zr-1Nb (α+β) intergranular hydrides seem to be observed (Fig. 6b). In Zr-1Nb α', the hydrides precipitated following the direction of the martensite neddles (Fig. 6c) and the same pattern seems to occur in aged Zr-1Nb α' (Fig. 6d). Fig. 6e shows the

hydride distribution characteristic of the circumferential-radial (CR) face of the PT: plates and bunches of hydrides preferentially oriented in the circumferential direction. In aged Zr-2.5Nb (PT), this special hydride distribution has disappeared; the hydrides are longer and some of them are oriented in the radial direction of the tube (Fig. 6f).

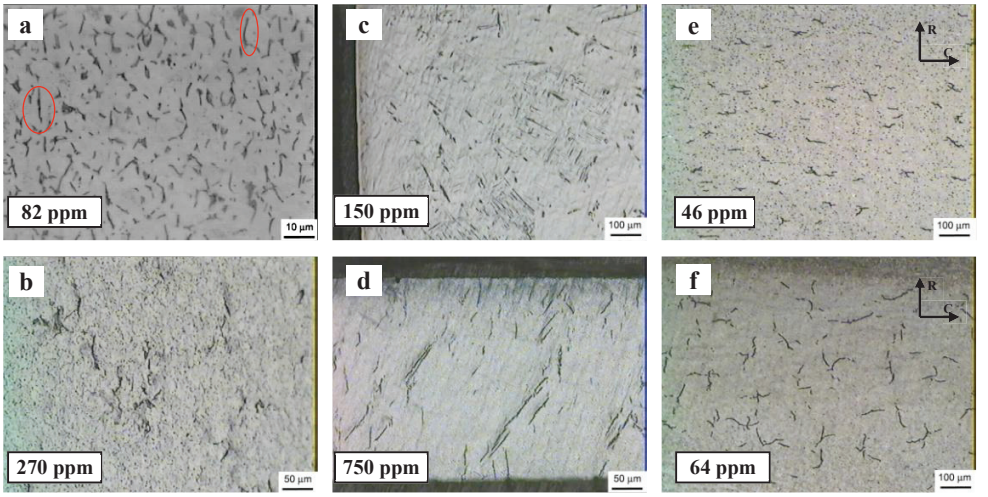

Fig. 6. Hydride distribution after ~ 14 days in 0.1 M LiOH at 343ºC: (a) Hydrides are marked in Zr-1Nb (α+β), (b) aged Zr-1Nb (α+β), (c) Zr-1Nb α', (d) aged Zr-1Nb α', (e) Zr-2.5Nb (PT), (f) aged Zr-2.5Nb (PT).

4. Discussion

The corrosion behavior of Zr-Nb alloys significantly depends on the microstructure, which can be modified by thermomechanical treatments. The α'-martensitic structures having niobium supersaturation in the matrix show poor corrosion resistance with the highest corrosion rates [Kim et al, 2004, Choo et al, 1994]. Moreover, it can be found in the literature that ageing treatments below the monotectoid temperature of 610°C improve the corrosion resistance of alloys with both α'-martensitic and (α-Zr+β-Zr) structures [Jeong et al, 2003, Kim et al, 2004, Choo et al, 1994]. It is not clear yet if the beneficial effect of ageing is due to the precipitation of small particles of equilibrium β-Nb phase (80 to 85% Nb) [Choo et al, 1994, Kim et al, (2005)] or to the presence of a α-Zr matrix with a niobium content close to the terminal solubility. The latter decreases with the presence of iron as an impurity, being ~ 0.6% Nb in alloys with low iron content (< 300 ppm) and ~ 0.2 % Nb for alloys with 700 ppm Fe [Kim et al, 2005]. In the present work, 4-months ageing treatments were performed at 560°C (Table 1), in order to achieve equilibrium compositions according to the data from the literature [Kim et al, 2005, Toffolon-Masclet et al, 2008].

After the ageing, the metastable β-Zr phase (~ 20% Nb) present in the Zr-2.5Nb (PT) was completely decomposed into α-Zr and β-Nb globular particles (Figs. 1e and 1f). The niobium content measured in these globules (~ 70 % Nb) (Fig. 2) was very close to the equilibrium value (~ 80 % Nb). Particles containing iron were not observed in aged Zr-2.5Nb, probably due to the low iron content of this alloy (~ 500 ppm).

Unlike Zr-2.5Nb (PT), precipitates of β-Nb, Zr-Nb-Fe and Zr-Fe (in minor proportion) were detected in aged Zr-1Nb (α+β), while β-Nb and Zr-Fe particles were observed in aged Zr-1Nb α'. The $Zr(Nb,Fe)_2$ phase was reported as an equilibrium phase in zirconium alloys with contents of : Nb > 0.3 % and Fe > 700 ppm [Kim et al, 2005, Toffolon-Masclet et al, 2008]. The fact that the Nb and Fe concentrations in the Zr-1Nb alloy studied in this work (~ 1.0 % Nb and ~1000 ppm Fe) are similar to those mentioned above, suggests that precipitates of Zr-Nb-Fe correspond to equilibrium phases in our alloy. Zr-Fe particles, which were detected in aged Zr-1Nb (α+β) and aged Zr-1Nb α', were not informed as equilibrium phases by Kim et al. (2005) and Toffolon-Masclet et al. (2008). Probably the EDS analysis used in the present work has not made it possible to find niobium in such small precipitates.

The corrosion kinetics in 0.1 M LiOH at 343ºC showed that all the Zr-Nb alloys suffered accelerated corrosion at

shorter testing times than the Zircaloy-4, which remained in the pre-transition regime during ~ 14 days in this medium (Fig. 3a). Then, it can be concluded that ageing of Zr-Nb alloys does neither affect the post-transition kinetics nor retard the transition.

The ageing improved the corrosion response in steam at 400°C (Fig. 3b), where the aged materials exhibited the lowest weight gains. Pre-transition oxides ($\Delta w \sim 20$ mg/dm^2) formed in water at 360°C in Zr-xNb alloys (x = 1 to 5 %) [Jeong et al, 2003, Kim et al, 2004] were reported to have a higher volume fraction of protective tetragonal ZrO_2 (present in the barrier layer) in aged materials than in non-aged ones. Jeong et al. (2003) observed that the β-Nb particles remained amorphous and partially oxidized in the columnar monoclinic ZrO_2 of aged alloys, while in non-aged materials the β-Zr phase was fully oxidized and developed a micro-equiaxed oxide structure. According to these authors, the β-Zr phase would accelerate the transformation from the columnar oxide to the equiaxed one (which is detrimental to the corrosion resistance) at the interface between β-Zr and surrounding oxide. They also thought that the β-Zr phase could favor the transformation from tetragonal ZrO_2 to monoclinic ZrO_2, while the β-Nb phase might not affect the oxide transformation. Choo et al. (1994) have suggested that a fine distribution of β-Nb precipitates inhibits the growth and recrystallization process of the oxide, thus improving the corrosion behavior of aged materials.

Zr-1Nb α' was the alloy with the lowest corrosion resistance in both media (Fig 3). In steam at 400°C, this material showed a linear kinetics from the beginning with $v_{corr} \sim 0.1$ mg/dm^{2}h, whereas in 0.1 M LiOH its corrosion rate was one order of magnitude higher ($v_{corr} \sim 2.2$ mg/dm^{2}h). According to the literature, the stresses and the niobium supersaturation present in the martensite matrix decrease the corrosion resistance of this metallurgical condition [Kim et al, 2004, Choo et al, 1994].

In 0.1 M LiOH solution, no particular ageing-effect was observed in the kinetics (Fig. 3a). Unlike the corrosion behavior observed in steam at 400°C, aged Zr-2.5Nb showed higher weight gains than those of non-aged Zr-2.5Nb. Nevertheless, the oxide formed on aged Zr-2.5Nb after ~ 14 days was more homogeneous and compact than that of the PT (Figs. 4e-4f and 5b-5c). It was reported that α-Zr/β-Zr interfaces have an important influence on the corrosion and on the appearance of oxides formed in both water [Cox, 2005] and LiOH solutions [Ding and Northwood, 1993]. The corrosion data obtained in the present work for Zr-2.5Nb (pre-transition region followed by a linear kinetics with $v_{corr} \sim 1$ mg/dm^{2}h) are in good agreement with data from the literature: for Zr-2.5Nb tested in 0.2 M LiOH at 300°C, Ding and Northwood (1993) reported weight gains fitting to the equation $\Delta w = at^{0.4}$ in the pre-transition, and a corrosion rate of ~ 0.9 mg/dm^{2}h for the linear post-transition regime. Comparing the oxide appearance and the H uptake (Table 2) for both Zr-2.5Nb alloys it can be inferred that, although ageing did not reduce the weight gains, the oxide integrity was improved due to the disappearance of the α-Zr/β-Zr interfaces. The presence of globulized β-Nb phase in aged Zr-2.5Nb avoided flaking of the oxide and did not affect the H uptake.

Unlike Zr-2.5Nb, ageing of Zr-1Nb (α+β) and Zr-1Nb α' produced β-Nb particles in coexistence with iron rich precipitates (Zr-Nb-Fe and Zr-Fe). These phases of complex crystal structures can absorb hydrogen [Cox, 1987], facilitating hydrogen entrance into the metal. Table 2 shows that aged Zr-1Nb (α+β) and aged Zr-1Nb α' have H uptake values of ~ 13%, which is three times higher than those obtained for the same materials without ageing (~ 4%). The H uptake for aged Zr-2.5Nb (3.1%), material in which iron-containing particles were not found, showed virtually no increase over that of Zr-2.5Nb (2.9%).

These experimental evidences lead us to infer that precipitates of Zr-Nb-Fe and Zr-Fe, which are present in our aged Zr-1Nb alloys, would be responsible for the increase in hydrogen uptake. Furthermore, the irregular size and inhomogeneous distribution of these particles (Fig. 1b-1d) would facilitate the hydrogen diffusion into the material [Hatano et al, 2000] and affect the oxide integrity, promoting oxide spalling as seen in aged Zr-1Nb (α+β). In a recent work, Choudhuri et al. (2013) studied the hydrogen absorption of Zr-2.5Nb with different iron contents (300, 800 and 1250 ppm Fe) autoclaved during three days in 415°C steam. They found that H uptake was doubled for tubes containing 1250 ppm Fe. According to these authors, the presence of Zr-Fe precipitates (and Zr-Nb-Fe in a lesser extent) facilitates the hydrogen absorption in the pressure tubes with high iron content.

Literature data show that hydrogen uptake considerably increases when zirconium alloys are in the post-transition period. In water autoclaving tests and pre-transition conditions, H uptakes of 10% - 20% were measured for Zircaloy-4, and of ~ 2% for Zr-2.5Nb (PT); in the post-transition, H uptake values of ~ 50% for Zircaloy-4 and of 15%-30% for Zr-2.5Nb were reported [Manolescu et al, 1982, Müller and Lanzani, 2013]. It can be seen in Fig. 3a that all Zr-Nb alloys exhibited post-transition kinetics from the second testing day in 0.1 M LiOH, which means that

the H uptakes obtained after ~ 14-day tests correspond to post-transition period. Comparing these values with those from the literature, it is observed that H uptakes for Zr-2.5Nb and aged Zr-2.5Nb are significantly low and close to those of pre-transition regime; the same happens for Zr-1Nb (α+β) and Zr-1Nb α'. Aged Zr-1Nb (α+β) and aged Zr-1Nb α' showed hydrogen uptakes around 13%, which is under the lower boundary measured for Zr-2.5Nb in the post-transition. These observations suggest that, even for high weight gains and for thick (sometimes deteriorated) oxides such as those formed in aged Zr-1Nb (α+β) and in Zr-2.5Nb, the Zr-Nb alloys show a good resistance to hydrogen entrance in such an aggressive medium as 0.1 M LiOH solution.

The behavior of Zircaloy-4 TREX in 0.1 M LiOH at 343°C has been better than that of the Zr-1Nb alloys (base material of M5 and ZIRLO alloys) after ~ 14-day test. However, there is no guarantee that this material does not undergo accelerated corrosion at longer test times. Kass (1969) found accelerated corrosion, with v_{corr} ~ 0.5 mg/dm^{2}h and H uptake of 42%, for Zircaloy-4 foils tested during ~ 10 days in 0.1 M LiOH at 316°C. The hydrogen uptake values reported in the literature for Zircaloy-4 in the post-transition both in water and in 0.1 M LiOH point out that, under post-transition conditions, the aged and non-aged Zr-1Nb alloys studied in the present work have a better behavior against hydrogen absorption than Zircaloy-4.

5. Conclusions

- 120-day ageing at 560ºC submitted to Zr-2.5Nb (~500 ppm Fe) and Zr-1Nb (~1000 ppm Fe) produced:
  a) globular precipitates of β-Nb aligned along the axial direction of the pressure tube.
  b) precipitates of variable size of β-Nb, Zr-Nb-Fe and Zr-Fe in both aged Zr-1Nb (α+β) and aged Zr-1Nb α'.
- In steam at 400ºC, the aged Zr-Nb alloys have a better corrosion behavior than the non-aged materials.
- The Zr-1Nb α' was the material with the poorest corrosion resistance, both in 0.1 M LiOH at 343ºC and in steam at 400ºC.
- The ageing of Zr-Nb alloys did not delay the breakaway in 0.1 M LiOH. In the case of Zr-2.5Nb (PT), the ageing did not decrease the weight gains, but it clearly improved the integrity of the oxide and did not affect the hydrogen uptake.
- The low hydrogen uptakes obtained for Zr-Nb alloys after 14 days in 0.1 M LiOH show that these alloys are highly resistant to hydrogen absorption, whatever the metallurgical condition. The presence of Zr-Nb-Fe and Zr-Fe precipitates in both aged Zr-1Nb (α+β) and aged Zr-1Nb α' seems to increase the hydrogen ingress.
- In post-transition conditions, the Zr-1Nb alloy exhibits a better behavior than Zircaloy-4 against the hydrogen absorption, independently of the microstructure.

Acknowledgements

The authors wish to thank Dr. Marta Granovsky for her valuable discussions about metallurgical structures of the alloys and Dr. Patricia Bozzano for the TEM observations. Thanks also due to Lic. María R. Eppis for the EDXRF analysis and Mr. Rubén Ríos for the hydrogen content determinations with a LECO® analyzer.

References

Cox, B., 2005. Some thoughts on the mechanisms of in-reactor corrosion of zirconium alloys. Journal of Nuclear Materials 336, 331-368.

Sabol, G., Kilp, G., Balfour, M., Roberts, E., 1989. ASTM STP 1023, 227.

Domizzi, G., Lanzani, L., Coronel, P., Bruzzoni, P., 1997. Supercharging of Zircaloy-4. Journal of Nuclear Materials 246, 247-251.

Manolescu, A., Mayer, P., Simpson, C., 1982. Effect of lithium hydroxide on corrosion rate of Zirconium-2.5Wt% Niobium in 340ºC water. Corrosion-NACE 38 Nº1, 23-31.

Kass, S., 1969. Corrosion and hydrogen pickup of Zircaloy in concentrated lithium hydroxide solutions. Corrosion- NACE 25 Nº1, 30-46.

Jeong, Y., Kim, H., Kim, T., 2003. Effect of β phase, precipitate and Nb-concentration in matrix on corrosion and oxide characteristic of Zr-*x*Nb alloys. Journal of Nuclear Materials 317, 1-12.

Kim, H., Jeong, Y., Kim, T., 2004. Effect of isothermal annealing on the corrosion behavior of Zr-xNb alloys. Journal of Nuclear Materials 326, 125-131.

Choo, K., Kang, Y., Pyun, S., Urbanic, V., 1994. Effect of composition and heat treatment on the microstructure and corrosion behavior of Zr-Nb alloys. Journal of Nuclear Materials 209, 226-235.

Urbanic, V., Chan, P., Khatamian, D., Woo, O., 1994. Growth and characterization of oxide films on Zircomium-Niobium alloys. Zirconium in the Nuclear Industry: Tenth International Symposium, ASTM STP 1245, Philadelphia, EEUU, p. 116-132.

Müller, S., Lanzani, L., 2013. Corrosion of Zirconium alloys in concentrated lithium hydroxide solutions. Journal of Nuclear Materials 439, 251-257.

Kim, H., Park, J., Jeong, Y., 2005. Phase boundary of the Zr-rich region in commercial grade Zr-Nb alloys. Journal of Nuclear Materials 347, 140-150.

Toffolon-Masclet, C., Guilbert, T., Brachet, J., 2008. Study of secondary intermetallic phase precipitation/dissolution in Zr alloys by high temperature-high sensitivity calorimetry. Journal of Nuclear Materials 372, 367-378.

Ding, Y., Northwood, D., 1993. Effects of LiOH on the microstructure of the oxide formed during the aqueous corrosion of a Zr-2.5wt%Nb alloy. Journal of Nuclear Materials 202, 180-192.

Cox, B., 1987. Zirconium intermetallics and hydrogen uptake during corrosion. AECL, Report NºAECL-9383.

Hatano, Y., Sugisaki, M., Kitano, K., Hayashi, M., 2000. Role of intermetallics precipitates in hydrogen transport through oxide films on Zircaloy. Zirconium in the Nuclear Industry: Twelfth International Symposium, ASTM STP 1354, West Conshohocken, PA, 901-917.

Choudhuri G., Jagannath, Kiran Kumar, M., Kain, V., Srivastava, D., Basu, S., Shah, B., Saibaba, N., Dey, G., 2013. Influence of Fe content on Corrosion and Hydrogen pickup behaviour of Zr-2.5Nb pressure tube material", Journal of Nuclear Materials, doi: http://dx.doi.org/10.1016/j.jnucmat.2013.05.026.